Chapter 4

Self Organization and Pattern Formation

Pattern formation occurs when complex spatio-temporal structures, like animal markings, result from seemingly simple dynamical evolution processes. Reaction-diffusion systems, like the Fisher equation, constitute in this context classical examples for the notion of self organization. A core concept for understanding the occurrence of non-trival spatio-temporal patterns is the Turing instability, which will be discussed together with the notion of self-stabilizing wavefronts.

Further prominent examples of self-organizing processes treated in this chapter involve collective decision making and swarm intelligence, as occurring in social insect and flocking birds, information offloading in terms of stigmergy, opinion dynamics and the physics of traffic flows, including the ubiquitous phenomenon of self-organized traffic congestions.

4.1 Interplay Between Diffusion and Reaction

Processes characterized by the random motion of particles or agents are said to be diffusive, compare Sect. **??**, and described by the diffusion equation

$$\frac{\partial}{\partial t}\rho(\mathbf{x},t) = D\Delta\rho(\mathbf{x},t), \qquad \Delta = \frac{\partial^2}{\partial x^2} + \frac{\partial^2}{\partial y^2} + \frac{\partial^2}{\partial z^2}\ , \tag{4.1}$$

with $D > 0$ denoting the diffusion constant, Δ the Laplace operator and $\rho(\mathbf{x},t)$ the density of walkers at any given point $(\mathbf{x},t)$ in space and time.

Reaction-Diffusion Systems The diffusion equation (4.1) describes conserving processes and the overall number of particles $\int d\mathbf{x}\rho(\mathbf{x},t)$ remains constant. With

$$\frac{\partial}{\partial t}\rho(\mathbf{x},t) = R(\rho)\ +\ D\Delta\rho(\mathbf{x},t) \tag{4.2}$$

one denote a *reaction-diffusion system*, where $R(\rho)$ constitutes the reaction of the system to the current state ρ. In biological settings ρ typically stands for the population density and $R(\rho)$ for reproduction processes, in the context of chemical reactions ρ is a measure for the relative concentration of a given substance whereas $R(\rho)$ functionally describes effective reaction rates.

Fisher Equation Considering a one-dimensional system and logistic growth for the reaction term one obtains the *Fisher equation*

$$\dot{\rho} = r\rho(1-\rho) \,+\, D\rho'', \qquad\qquad \rho \in [0,1] \ , \tag{4.3}$$

which describes a reproductive and diffusive species in an environment with spatially local resource limitation.

Normal Form All one-component reaction-diffusion equations can be cast into a dimensionless normal form, by rescaling the time and space coordinates appropriately via

$$t = \alpha\tilde{t}, \qquad\qquad x = \beta\tilde{x}, \qquad\qquad \frac{\partial}{\partial t} = \frac{1}{\alpha}\frac{\partial}{\partial \tilde{t}}, \qquad\qquad \frac{\partial^2}{\partial x^2} = \frac{1}{\beta^2}\frac{\partial^2}{\partial \tilde{x}^2} \ ,$$

which leads to, for the Fisher equation (4.3),

$$\frac{\partial \rho}{\partial \tilde{t}} = \alpha r\rho(1-\rho) + \frac{\alpha D}{\beta^2}\frac{\partial^2 \rho}{\partial \tilde{x}^2}, \qquad\qquad \alpha r = 1, \qquad\qquad \frac{\alpha D}{\beta^2} = 1 \ .$$

It is hence sufficient to consider the normal form

$$\dot{\rho} = \rho(1-\rho) \,+\, \rho'' \tag{4.4}$$

of the Fisher equation.

Saturation and Wavefront Propagation The reaction term $R(\rho) = \rho(1-\rho)$ of the Fisher equation is strictly positive for $\rho \in [0,1]$ and hence

$$\lim_{t\to\infty} \rho(x,t) = 1 \ ,$$

viz the system saturates. The question of interest is however how saturation is achieved when starting from a local population $\rho(x,0)$, a simulation is presented in Fig. 4.1. The system develops wavefronts with a characteristic shape and velocity. In a biological setting this corresponds to an expansion wave allowing an initial local population to invade ballistically the uninhabited regions of the surrounding ecosystem.

This is an interesting observation, since diffusion processes alone (in the absence of a reaction term) would lead only to an expansion $\sim \sqrt{t}$, see Sect. **??**, whereas ballistic propagation is linear in time.

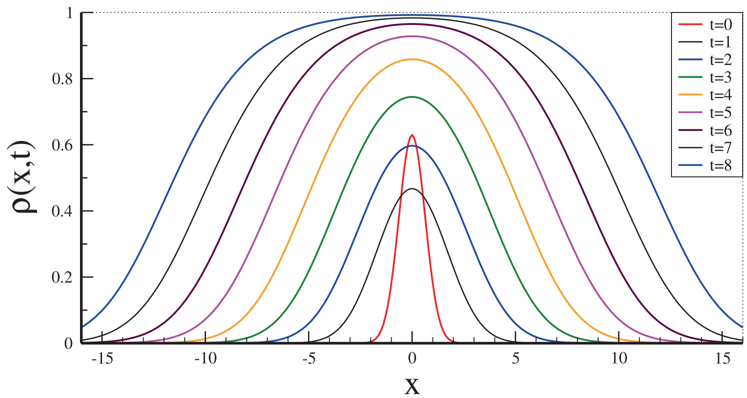

Fig. 4.1 Simulation of the Fisher reaction-diffusion equation (4.4). Plotted is $\rho(x,t)$ for $t = 0,\dots,8$. For the initial distribution $\rho(x,0)$ a Gaussian has been taken, which does not correspond to the natural line-form, but already at $t = 1$ the system has relaxed. The wavefronts propagate asymptotically with velocities ± 2

4.1.1 Travelling Wavefronts in the Fisher Equation

In order to describe the propagation of wavefronts in a diffusion-reaction system we consider shape-invariant propagating solutions of the form

$$\rho(x,t) = u(x-ct), \qquad \dot\rho = -cu', \qquad \rho'' = u'' \ . \tag{4.5}$$

This ansatz leads, for the Fisher equation (4.4), to the two-component ordinary differential equation

$$u'' + cu' + u(1-u) = 0, \qquad \left\{ \begin{array}{l} u' = v \\ v' = -cv - u(1-u) \end{array} \right\} , \tag{4.6}$$

with fixpoints $\mathbf{u}^* = (u^*, v^*)$,

$$\mathbf{u}_0^* = (0,0), \qquad \mathbf{u}_1^* = (1,0) \ . \tag{4.7}$$

Minimal Propagation Velocity For the stability of the trivial fixpoint $\mathbf{u}_0^* = (0,0)$ one expands (4.6) for small (u,v),

$$\begin{pmatrix} u' \\ v' \end{pmatrix} = \begin{pmatrix} 0 & 1 \\ -1 & -c \end{pmatrix} \begin{pmatrix} u \\ v \end{pmatrix}, \qquad \lambda(\lambda + c) + 1 = 0 \ ,$$

where λ is an eigenvalue of the Jacobian (see also Sect. **??**), given by

$$\lambda_\pm = \frac{1}{2}\left(-c \pm \sqrt{c^2-4}\right), \qquad c \geq 2 \ . \tag{4.8}$$

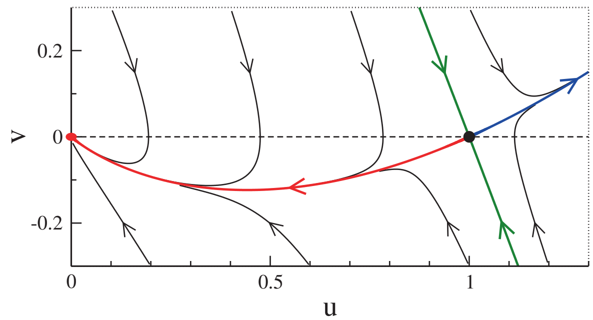

Fig. 4.2 Phase space trajectories of the travelling-wave solution $\rho(x,t) = u(z)$, with $z = x - ct$ and $v = u'$, as determined by (4.6). The shape of the propagating wavefront is determined by the heteroclinic trajectory emerging from the saddle $(1,0)$ and leading to the stable fixpoint $(0,0)$

A complex eigenvalue would lead to a spiral around $\mathbf{u}_0^* = (0,0)$, which is not possible since $u \in [0,1]$ is strictly positive. Hence $c = 2$ is the minimal occurring propagation velocity. The trivial fixpoint $(0,0)$ is stable, since $\sqrt{c^2-4} < c$ for $c \geq 2$ and hence $\lambda_\pm < 0$ (Fig. 4.2).

Saddle Restpoint The eigenvalues of the $\mathbf{u}_1^* = (1,0)$ are given by

$$\frac{d}{dz}\begin{pmatrix} u-1 \\ v \end{pmatrix} = \begin{pmatrix} 0 & 1 \\ 1 & -c \end{pmatrix}\begin{pmatrix} u-1 \\ v \end{pmatrix}, \qquad \lambda_\pm = \frac{1}{2}\left(-c \pm \sqrt{c^2+4}\right) ,$$

when denoting $u = u(z)$. The fixpoint $(1,0)$ is hence a saddle, with $\lambda_- < 0$ and $\lambda_+ > 0$. The unstable direction $u^*(z)$, emerging from the saddle and leading to the stable fixpoint $(0,0)$ (viz the heteroclinic trajectory) is the only trajectory in phase space fulfilling the conditions

$$\lim_{z\to-\infty} u^*(z) = 1, \qquad \lim_{z\to\infty} u^*(z) = 0, \qquad \lim_{z\to\pm\infty} v^*(z) = 0 \tag{4.9}$$

characterizing a propagating wavefront. The lineshape $u^*(z)$ of the wavefront can be evaluated numerically, see Fig. 4.3.

Exact Particular Solution of the Fisher Equation A special travelling-wave solution for the Fischer equation (4.4) is given by

$$\rho^*(x,t) = \sigma^2(x-ct), \qquad \sigma(z) = \frac{1}{1+\mathrm{e}^{\beta z}} \tag{4.10}$$

where $\sigma(\beta z)$ is called *sigmoidal* or *Fermi function*. It's derivatives are

$$\sigma' = \frac{-\beta \mathrm{e}^{\beta z}}{(1+\mathrm{e}^{\beta z})^2} = -\beta\sigma(1-\sigma), \qquad \sigma'' = \beta^2(1-2\sigma)\sigma(1-\sigma) , \tag{4.11}$$

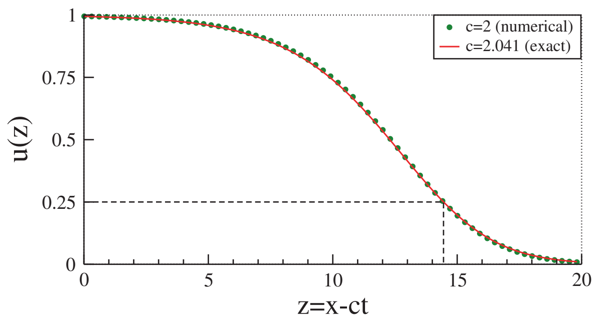

Fig. 4.3 Numerical result for the minimal velocity ($c = 2$) wavefront solution $u^*(z)$, compare Eq. 4.9, of the Fisher reaction-diffusion equation (4.4). For comparison the wavefront for a slightly larger velocity $c = 5/\sqrt{6} \approx 2.041$ has been plotted, for which the shape can be obtained analytically, see Eq. (4.10). The *dashed lines* indicates $u = 1/4$, which has been used to align the respective horizontal offsets

and hence

$$\frac{\partial \rho^*}{\partial t} = 2c\beta\sigma^2(1-\sigma), \qquad \frac{\partial^2 \rho^*}{\partial x^2} = \frac{\partial}{\partial x}(-2\beta\sigma^2)(1-\sigma) = \beta^2(4\sigma-6\sigma^2)\sigma(1-\sigma)\ .$$

The solution ρ^* fulfills the Fisher equation,

$$\frac{\partial \rho^*}{\partial t} - \frac{\partial^2 \rho^*}{\partial x^2} = \sigma^2(1-\sigma)\underbrace{\left[2c\beta - \beta^2(4-6\sigma)\right]}_{\stackrel{!}{=}(1+\sigma)} \stackrel{!}{=} \sigma^2(1-\sigma^2) \equiv \rho^*(1-\rho^*)\ ,$$

if

$$1 = 6\beta^2, \qquad 1 = 2c\beta - 4\beta^2 = 2c\beta - \frac{4}{6}, \qquad 2c\beta = \frac{10}{6} = \frac{5}{3}\ ,$$

which determines the two free parameters β and c as

$$\beta = \frac{1}{\sqrt{6}}, \qquad c = \frac{5}{6\beta} = \frac{5}{\sqrt{6}} \approx 2.041\ , \tag{4.12}$$

with the propagation velocity c of $\rho^*(x,t)$ being very close to the lower bound $c = 2$ for the allowed velocities. The resulting lineshape is nearly identical to the numerically-obtained minimal-velocity shape for the propagating wavefront, as shown in Fig. 4.3.

Exponential Falloff of Wavefronts The population density $\rho(x,t) = u(z)$ become very small for large $z = x - ct$ an and the quadratic term in (4.6) may be neglected,

$$u'' + cu' + u \approx 0,$$

with the solution

$$u(z) = \mathrm{e}^{-az}, \qquad a^2 - ca + 1 = 0, \qquad c = a + \frac{1}{a}\ . \tag{4.13}$$

The forward tails of all propagating are hence exponential, with the minimal velocity c corresponding to $a = 1$. Relation (4.13) holds also the exact solution (4.10), for which $a = 2\beta$,

$$c = \frac{1}{2\beta} + 2\beta = \frac{1+4\beta^2}{2\beta} = \frac{6+4}{2\sqrt{6}} = \frac{5}{\sqrt{6}}\ ,$$

in agreement with (4.12), when using $\beta = 1/\sqrt{6}$.

4.1.2 Sum Rule for the Shape of the Wavefront

The travelling-wave equation (4.6),

$$c(u')^2 = -\big(u(1-u)+u''\big)u', \qquad \lim_{z\to\infty} u(z) = 0, \qquad \lim_{z\to-\infty} u(z) = 1\ , \tag{4.14}$$

may be used to derive a sum rule for the shape $u(z)$ of the wavefront by integrating (4.14),

$$c\int_{-\infty}^{z} \big(u'(w)\big)^2 dw = A + \frac{u^3(z)}{3} - \frac{u^2(z)}{2} - \frac{\big(u'(z)\big)^2}{2}\ . \tag{4.15}$$

The integration constant A is determined by considering $z \to -\infty$ and taking into account that $\lim_{z\to\pm\infty} u'(z) = 0$,

$$A = \frac{1}{2} - \frac{1}{3} = \frac{1}{6}, \qquad \int_{-\infty}^{\infty} \big(u'(w)\big)^2 dw = \frac{1}{6c}\ , \tag{4.16}$$

where the second equation is the sum rule for u'. The wavefront is steepest for the minimal velocity $c = 2$.

Sum rule for Generic Reaction Diffusion Systems Sum rules equivalent to (4.16) can be derived for any integrable reaction term $R(\rho)$ in (4.2). One finds, by generalizing the derivation leading to (4.16),

$$\int_{-\infty}^{\infty} \big(u'(w)\big)^2 dw = \frac{1}{c}\int_0^1 R(\rho)d\rho\ . \tag{4.17}$$

In biological setting the reaction term corresponds to the reproduction rate. It is hence generically non-negative, $R(\rho) \ge 0$ and the right-hand side of the sum rule (4.17) positive. Note, that the diffusion constant D has no influence on the sum rule.

Sum rule for the Exact Particular Solution We verify that the sum rule (4.16) for the Fisher equation is satisfied by the special solution (4.10),

$$u_*(z) = \sigma^2(z), \qquad \sigma(z) = \frac{1}{1+\mathrm{e}^{\beta z}} \qquad \sigma' = -\beta\sigma(1-\sigma)\ .$$

With $u_*' = -2\beta\sigma^2(1-\sigma)$ we integrate

$$\int_{-\infty}^{\infty} \big(u_*'(w)\big)^2 dw = \int_{-\infty}^{\infty} (-4\beta)\sigma^3(1-\sigma)\underbrace{(-\beta)\sigma(1-\sigma)}_{\sigma'} dw$$
$$= 4\beta\left(\frac{1}{4}-\frac{1}{5}\right) = \frac{\beta}{5} = \frac{\beta^2}{5\beta} = \frac{1}{6c}\ ,$$

where we have used $\beta^2 = 1/6$ and $c = 5\beta$, see (4.12). Note that only the lower bound $z \to -\infty$ contributes to above integral.

4.1.3 Self-Stabilization of Travelling Wavefronts

The Fisher equation $\dot\rho = \rho(1-\rho)+\rho''$ supports travelling wavefront solutions $\rho(x,t) = u(x-ct)$ for any velocity $c \geq 2$. The observed speed of a wavefront may either depend on the starting configuration $\rho(x,0)$ or may self-organize to a universal value. We use perturbation theory in order to obtain an heuristic insight into this issue.

Solution of the Linearized Fischer Equation The solution of the linearized Fischer equation

$$\dot\rho = r\rho\ +\ \rho'', \qquad r = 1 \tag{4.18}$$

can be constructed for arbitrary initial conditions $p_0(x) = \rho(x,0)$ and is given for $r = 0$ by the solution of the diffusion equation,

$$\rho_0(x,t) = \int dy\, \Phi(x-y,t)\, p_0(y), \qquad \Phi(x,t) = \frac{1}{\sqrt{4\pi t}}\mathrm{e}^{-x^2/(4t)}\ , \tag{4.19}$$

with $\lim_{t\to 0}\Phi(x,t) = \delta(x)$, see Sect. **??**. For $r = 1$ the solution of (4.18) is

$$\rho(x,t) = \mathrm{e}^t\rho_0(x,t), \qquad \rho(x,0) = p_0(x)\ , \tag{4.20}$$

corresponding to an exponentially growing diffusive behavior.

Velocity Stabilization and Self Organization The kernel of (4.20)

$$\mathrm{e}^t\Phi(x,t) \propto \mathrm{e}^{-x^2/(4t)+t} = \mathrm{e}^{-(x^2-4t^2)/(4t)} = \mathrm{e}^{-(x-2t)(x+2t)/(4t)} \tag{4.21}$$

has a left- and a right propagating front travelling with propagation speeds $c = \pm 2$. The envelopes of the respective wavefronts are time dependent and do not show the simple exponential tail (4.13), as exponential falloffs are observed only for solutions $\rho(x,t) = u(x-ct)$ characterized by a single velocity c.

- *Ballistic Transport*
  The expression (4.21) shows that the interplay between diffusion and exponential growth, the reaction of the system, leads to ballistic transport.
- *Velocity Selection*
  The perturbative result (4.21) indicates, that the minimal velocity $|c| = 2$ is achieved for the wavefront when starting from an arbitrary localized initial state $p_0(x)$, since $\lim_{t\to 0} \mathrm{e}^t \Phi(x,t) = \delta(x)$.
- *Self Organization*
  Propagating wavefronts with any $c \geq 2$ are stable solutions of the Fisher equation, but the system settles to $c = 2$ for localized initial conditions. The stabilization of a non-trivial dynamical property for a wide range of starting conditions may be considered as an example of *self organization*.

Above considerations did regard the speed c of the travelling wavefront, but do not make any direct statement regarding the lineshape.

Stability Analysis of the Wavefront In order to examine the stability of the shape of the wavefront we consider

$$\rho(x,t) = u(z) \,+\, \epsilon\psi(z)\mathrm{e}^{-cz/2}\mathrm{e}^{-\lambda t}, \qquad\qquad z = x - ct \;, \tag{4.22}$$

where the second term with $\epsilon \ll 1$ is a perturbation to the solution $u(z)$ of the travelling wave equation (4.6). The derivatives are

$$\begin{aligned}
\dot\rho &= \; -cu' + \epsilon\big[(c^2/2-\lambda)\psi - c\psi'\big]\mathrm{e}^{-cz/2}\mathrm{e}^{-\lambda t} \\
\rho' &= \; u' + \epsilon\big[-c\psi/2 + \psi'\big]\mathrm{e}^{-cz/2}\mathrm{e}^{-\lambda t} \\
\rho'' &= \; u'' + \epsilon\big[c^2\psi/4 - c\psi' + \psi''\big]\mathrm{e}^{-cz/2}\mathrm{e}^{-\lambda t}
\end{aligned}$$

and we find

$$\begin{aligned}
\dot\rho - \rho'' &= -\big[cu' + u''\big] \,+\, \epsilon\big[(c^2/4-\lambda)\psi - \psi''\big]\mathrm{e}^{-cz/2}\mathrm{e}^{-\lambda t} \\
\rho(1-\rho) &\approx u(1-u) \,+\, \epsilon\big[1-2u\big]\psi\mathrm{e}^{-cz/2}\mathrm{e}^{-\lambda t} \;.
\end{aligned}$$

Wavefront Self-Stabilization With above results the Fisher equation $\dot\rho - \rho'' = \rho(1-\rho)$ reduces to

$$\left[-\frac{d^2}{dz^2} \,+\, V(z)\right]\psi(z) = \lambda\psi(z), \qquad\qquad V(z) = 2u(z) + \frac{c^2}{4} - 1 \;, \tag{4.23}$$

to order $O(\epsilon)$. This expression corresponds to a time-independent one-dimensional Schrödinger equation for a particle with a mass $m = \hbar^2/2$ moving in a potential

$$V(z) \;\geq\; 0, \qquad \text{for} \qquad c \geq 2\,.$$

The potential $V(z)$ is strictly positive since $u(z) \in [0,1]$ and the eigenvalues λ are hence also positive. The perturbation term in (4.22) consequently decays with $t \to \infty$ and the wavefront self-stabilizes.

This result would be trivial if it would be known a priori that the wavefront equation $u'' + cu' + u(1-u) = 0$ has a unique solution $u(z)$. In this case all states of the form of (4.22) would need to contract to $u(z)$. The stability condition (4.23) indicates that the travelling-wavefront solutions to the Fisher equation may be indeed unique.

4.2 Interplay Between Activation and Inhibition

In chemical reaction systems one reagent may activate or inhibit the production of the other components, leading to non-trivial chemical reaction dynamics. Chemical reagents typically also diffuse spatially and the interplay between the diffusion process and the chemical reaction dynamics may give rise to the development to spatially structured patterns.

4.2.1 Turing Instability

The reaction-diffusion system (4.2) contains additively two terms, the reaction and the diffusion term. Diffusion alone leads generically to an homogeneous steady state.

For the reaction terms considered in Sect. 4.1 the reference state $\rho = 0$ was unstable against perturbations. Will now consider reaction terms for which the reference homogeneous state is however stable. Naively one would expect a further stabilization of the reference state, but this is not necessarily the case.

Turing instability. The interaction of two processes, which separately would stabilize a given homogeneous reference state, can lead to an instability.

The Turing instability is thought to be the driving force behind the formation of spatio-temporal patterns observed in many physical and biological settings, such as the stripes of a zebra.

Turing Instability of Stable Oscillators As a first example we consider a linear two-dimensional dynamical system composed of two stable oscillators,

$$\dot{\mathbf{x}} = A\mathbf{x}, \qquad A_1 = \begin{pmatrix} -\epsilon_1 & 1 \\ -a & -\epsilon_1 \end{pmatrix}\,, \qquad A_2 = \begin{pmatrix} -\epsilon_2 & -a \\ 1 & -\epsilon_2 \end{pmatrix}\,. \tag{4.24}$$

Here $0 < a < 1$ and $\epsilon_\alpha > 0$, for $\alpha = 1, 2$. The eigenvalues for the matrices A_α and $A = A_1 + A_2$ are

$$\lambda_\pm(A_\alpha) = -\epsilon_\alpha \pm i\sqrt{a}, \qquad \lambda_\pm(A) = -(\epsilon_1 + \epsilon_2) \pm (1 - a) \ .$$

The origin of the system $\dot{\mathbf{x}} = (A_1 + A_2)\mathbf{x}$ hence becomes a saddle if $1 - a > \epsilon_1 + \epsilon_2$, an instance of a Turing instability: Superposing two stable vector fields may generate unstable directions.

Eigenvalues of Two-Dimensional Matrices We remind ourselves that the eigenvalues $\lambda_\pm$ of a 2×2 matrix A can be written in terms of the trace $a + b$ and of the determinant $\Delta = ab - cd$,

$$A = \begin{pmatrix} a & d \\ c & b \end{pmatrix} \ , \qquad \lambda_\pm = \frac{a+b}{2} \pm \frac{1}{2}\sqrt{(a+b)^2 - 4\Delta} \ . \tag{4.25}$$

For negative determinants $\Delta < 0$ the system has both an attracting and a repelling eigenvalue, when using the terminology suitable for the classification of fixpoints, compare Sect. **??**.

Superposing a Stable Node and a Stable Focus We now consider what may happen when superimposing a stable node and a stable focus, the later being defined as

$$A_1 = \begin{pmatrix} -\epsilon_a & 1 \\ -1 & \epsilon_b \end{pmatrix} \ , \qquad \Delta_1 = 1 - \epsilon_a\epsilon_b > 0, \qquad (\epsilon_b - \epsilon_a)^2 < 4\Delta_1 \ . \tag{4.26}$$

with $\epsilon_a > \epsilon_b > 0$. The system $\dot{\mathbf{x}} = A_1\mathbf{x}$ is then a stable focus when the trace $\epsilon_b - \epsilon_a < 0$ is negative, compare Eq. (4.25), having two complex conjugate eigenvalues with a negative real part. Possible values are, e.g. $\epsilon_a = 1/2$ and $\epsilon_b = 1/4$.

We now add a stable node

$$A_2 = \begin{pmatrix} -a & 0 \\ 0 & -b \end{pmatrix} \ , \qquad A = \begin{pmatrix} -\epsilon_a - a & 1 \\ -1 & \epsilon_b - b \end{pmatrix} \ . \tag{4.27}$$

Can we select $a, b > 0$ such that $A = A_1 + A_2$ becomes a saddle? The determinant Δ of A

$$1 - (\epsilon_a + a)(\epsilon_b - b)$$

should then become negative, compare Eq. (4.25). This is clearly possible for $b < \epsilon_b$ and a large enough a.

Turing Instability and Activator-Inhibitor Systems The interplay of one activator and one inhibitor often results in a stable focus, as described by (4.26). Diffusion processes correspond, on the other side, to stable nodes, such as A_2 in Eq. (4.27). The Turing instability possible when superimposing a stable node and a stable focus is hence of central relevance for chemical reaction-diffusion systems.

4.2.2 Pattern Formation

We now consider a generic reaction-diffusion system of type (4.2)

$$\begin{aligned}\dot{\rho} &= f(\rho,\sigma) + D_\rho \Delta\rho \\ \dot{\sigma} &= g(\rho,\sigma) + D_\sigma \Delta\sigma\end{aligned} \tag{4.28}$$

containing two interacting components, $\rho = \rho(\mathbf{x},t)$ and $\sigma = \sigma(\mathbf{x},t)$, characterized by respective diffusion constants D_ρ, $D_\sigma > 0$. We assume, that the reaction system $\mathbf{R} = (f,g)$ has a stable homogeneous solution with steady-state densities ρ_0 and σ_0 respectively, together with the stability matrix

$$A_1 = \begin{pmatrix} f_\rho & f_\sigma \\ g_\rho & g_\sigma \end{pmatrix}, \qquad g_\rho f_\sigma < 0, \qquad f_\rho + g_\sigma < 0 \tag{4.29}$$

which we assume to model an activator-inhibitor system characterized by $g_\rho f_\sigma < 0$. Here $f_\rho = \partial f/\partial\rho$, etc, denotes the relevant partial derivatives. We may always rescale the fields ρ and σ such that $|g_\rho| = 1 = |f_\sigma|$ and (4.29) is then identical with the previously used representation (4.26).

Fourier Expansion of Perturbations The reaction term $\mathbf{R} = (f,g)$ is independent of $\mathbf{x}$ and we may hence expand the perturbation of the fields around the equilibrium state in term of spatial Fourier components. Equivalently we consider with

$$\begin{aligned}\rho(\mathbf{x},t) &= \rho_0 \,+\, \mathrm{e}^{-i\mathbf{k}\cdot\mathbf{x}}\,\delta\rho(t) \\ \sigma(\mathbf{x},t) &= \sigma_0 \,+\, \mathrm{e}^{-i\mathbf{k}\cdot\mathbf{x}}\,\delta\sigma(t)\end{aligned} \tag{4.30}$$

a single harmonic deviation from the equilibrium state (ρ_0, σ_0). We obtain

$$\begin{pmatrix} \delta\dot{\rho} \\ \delta\dot{\sigma} \end{pmatrix} = A \begin{pmatrix} \delta\rho \\ \delta\sigma \end{pmatrix}, \qquad A_2 = \begin{pmatrix} -D_\rho k^2 & 0 \\ 0 & -D_\sigma k^2 \end{pmatrix}, \tag{4.31}$$

where the overall stability matrix $A = A_1 + A_2$ is given by the linear superposition of a stable focus A_1 and a stable node A_2.

Spatio-Temporal Turing instability For concreteness we assume now that $f_\rho < 0$ and $g_\sigma > 0$, in analogy with (4.26), together with $0 > g_\sigma f_\rho = -|g_\sigma f_\rho|$. The determinant Δ of A is then

$$\Delta = |f_\sigma g_\rho| - \big(|f_\rho| + D_\rho k^2\big)\big(|g_\sigma| - D_\sigma k^2\big)\ . \tag{4.32}$$

A Turing instability occurs when the determinant Δ becomes negative, which is possible if the respective diffusion constants D_ρ and D_σ are different in magnitude.

– When the determinant (4.32) is reduced the homogeneous fixpoint solution changes first from a stable focus to a stable node as evident from

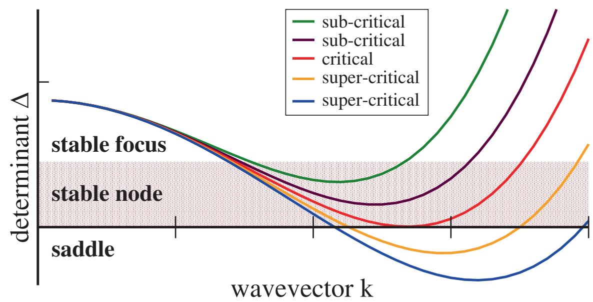

Fig. 4.4 The determinant Δ of the Turing bifurcation matrix, see Eq. (4.32), for a range $d = D_\sigma/D_\rho$ of ratios of the two diffusion constants. For large $d \to 1$ the determinant remains positive, becoming negative for a finite interval of wavevectors k when d becomes small enough. With decreasing size of the determinant the fixpoint changes from a stable focus (two complex conjugate eigenvalues with negative real components) to a stable node (two negative real eigenvalues) and to a saddle (a real positive and a real negative eigenvalue), compare Eq. (4.25)

expression (4.25). The instability at $\Delta = 0$ is hence a transition from a stable focus to a saddle, as illustrated in Fig. 4.4.
– The contribution A_2 of the diffusion induces the transition and can be hence regarded as a bifurcation parameter.

Diffusion processes may act as bifurcation parameters also within other bifurcation scenarios, like a Hopf bifurcation, as we will discuss in more detail in Sect. 4.2.3.

Mode Competition For a real-world chemical reaction system the parameters are fixed and a range of Fourier modes with a negative determinant (4.32), and corresponding positive Lyapunov exponents (4.25), will start to grow and compete with each others. The shape of the steady-state pattern, if any, will be determined in the end by the non-linearities of the reaction term.

4.2.3 The Gray-Scott Reaction Diffusion System

Several known examples of reaction-diffusion models showing instabilities towards the formation of complex spatio-temporal patterns are characterized by contributions $\pm\rho\sigma^2$ to the reaction term,

$$\begin{aligned} \dot\rho &= -\rho\sigma^2 + F(1-\rho) + D_\rho\Delta\rho \\ \dot\sigma &= \quad \rho\sigma^2 - (F+k)\sigma + D_\sigma\Delta\sigma \end{aligned} \tag{4.33}$$

corresponding to a chemical reaction needing two σ-molecules and one ρ-molecule. The remaining contributions to the reaction term in (4.33) serves for the overall mass balance, which can be implemented in various ways. In Eq. (4.33) the *Gray-Scott* system is given, a slightly different choice for the mass conservation terms would lead to the *Brusselator* model. The replenishment rate for the reactant $\rho < 1$ is given by F, with σ being lost to the environment at a rate $K = F + k$.

Saddle-Node Bifurcation The three fixpoints of the reaction term of Gray-Scott system (4.33) are $\mathbf{p}_i^* = (\rho_i^*, \sigma_i^*)$, with $\mathbf{p}_0^* = (1,0)$ and

$$\rho_i^* \sigma_i^* \;=\; K, \qquad F\rho_i^* + K\sigma_i^* \;=\; F, \qquad i \;=\; 1,\, 2\;. \tag{4.34}$$

These fixpoint conditions lead to

$$\rho_{1,2}^* \;=\; (1 \pm a)/2, \qquad \sigma_{1,2}^* \;=\; (1 \mp a)F/(2K), \qquad a = \sqrt{1 - 4K^2/F}\;.$$

The trivial fixpoint $\mathbf{p}_0^*$ has a diagonal Jacobian with eigenvalues $-F$ and $-K$ respectively. It is always stable, even in the presence of diffusion. For

$$F \;>\; 4K^2 = 4(k+F)^2, \qquad k_c = \sqrt{F_c}/2 - F_c\;, \tag{4.35}$$

and positive k, only $\mathbf{p}_0^*$ exists and a saddle-node bifurcation occurs along the critical line (k_c, F_c), when $a \to 0$ and $\mathbf{p}_1^*$ and $\mathbf{p}_2^*$ merge and annihilate each other. Compare Fig. 4.5 and Sect. **??**.

The Saddle Fixpoint $\mathbf{p}_1^*$ The non-trivial restpoints $\mathbf{p}_{1,2}^*$ have the Jacobian and the determinants

$$\begin{pmatrix} -(F + (\sigma_{1,2}^*)^2) & -2K \\ (\sigma_{1,2}^*)^2 & K \end{pmatrix}, \qquad \begin{aligned} \Delta_{1,2} &= K\left((\sigma_{1,2}^*)^2 - F\right) \\ &= KF\left((\sigma_{1,2}^*)^2/F - 1\right) \end{aligned}\;. \tag{4.36}$$

The determinants $\Delta_{1,2}$ can be written as

$$\frac{\Delta_{1,2}}{KF} = \left(\frac{1 \mp \sqrt{1 - 4\gamma^2}}{2\gamma}\right)^2 - 1, \qquad \gamma \;=\; \frac{K}{\sqrt{F}} \;\in\; [0, 1/2]\;. \tag{4.37}$$

The non-trivial fixpoints exists for $0 < \gamma^2 < 1/4$ and Δ_1 is always negative, $\mathbf{p}_1^*$ is hence always a saddle.

Focus Transition for $\mathbf{p}_2^*$ The focus $\mathbf{p}_2^*$ changes from stable to unstable when the trace

$$K_f - F_f - (\sigma_2^*)^2 \;=\; 0, \qquad \sigma_2^* \;=\; \sqrt{K_f - F_f} \;=\; \sqrt{k_f}, \tag{4.38}$$

of the Jacobian (4.36) of $\mathbf{p}_2^*$ changes along the line (k_f, F_f). Using the fixpoint conditions (4.34)

$$\frac{K}{\sigma_2^*} \;=\; \rho_2^* \;=\; 1 - \frac{K}{F}\sigma_2^*, \qquad K\,\frac{F + (\sigma_2^*)^2}{F} \;=\; \sigma_2^*\;,$$

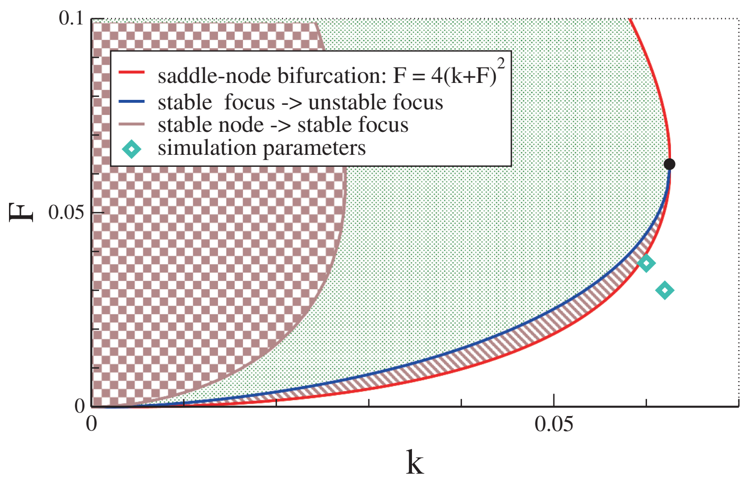

Fig. 4.5 Phase diagram for the reaction term of the Gray-Scott model (4.33). Inside the saddle-node bifurcation line (*solid red line*), see Eq. (4.35) there are three fixpoints $\mathbf{p}_i^*$ $(i = 0, 1, 2)$, outside the saddle-node bifurcation line only the stable trivial restpoint $\mathbf{p}_0^*$ is present. $\mathbf{p}_1^*$ is a saddle and $\mathbf{p}_2^*$ a stable node (*checkerboard brown area*), a stable focus (*light shaded green area*) or an unstable focus (*shaded brown area*), the later two regions being separated by the focus transition line (*solid blue line*), as defined by (4.39). The *black filled circle* denotes $\mathbf{p}_c = (1, 1)/16$. and the open diamonds the parameters used for the simulation presented in Fig. 4.7

$K = k + F$ and (4.38), we obtain

$$(F_f + k_f)^2 = F_f \sqrt{k_f} \tag{4.39}$$

for the focus transition line (k_f, F_f). One can verify that the Lyapunov exponents are complex along (4.39), becoming however real for lower values of k, as illustrated in Fig. 4.5. The endpoint of (4.39) is

$$\mathbf{p}_c = (1/16, 1/16) = (0.0625, 0.0625) \ , \tag{4.40}$$

in the (k, F) plane, which coincides with the turning point of the saddle-node line (4.35).

Merging of an Unstable Focus and a Saddle In Fig. 4.6 we illustrate the flow of the reaction term of the Gray-Scott model for two sets of parameters (k, F). The unstable focus $\mathbf{p}_2^*$ and the saddle $\mathbf{p}_1^*$ annihilate each other for $k \to k_c$. One observes that the large-scale features of the flow are remarkable stable similar for $k < k_c$ and $k > k_c$, as all trajectories, apart from the stable manifolds of the saddle, flow to the global attractor $\mathbf{p}_0^* = (1, 0)$.

Attractor Relict Dynamics Close to the outside of the saddle-node line (k_c, F_c) the dynamics slows down when approaching a local minimum of

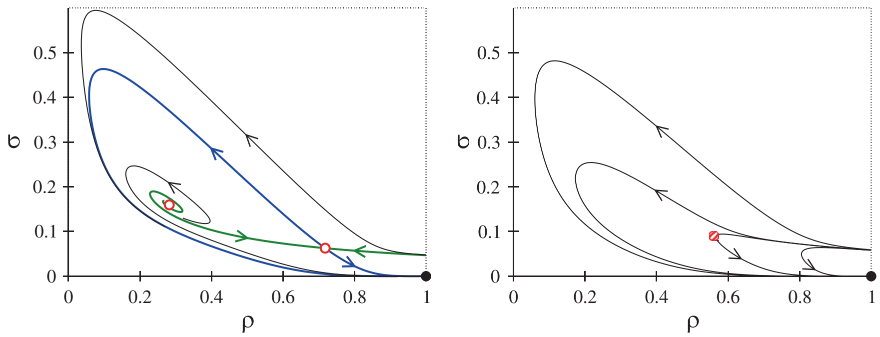

Fig. 4.6 Flow of the reaction term of the Gray-Scott model (4.33) in phase space (ρ,σ), for $F = 0.01$. The stable fixpoint $\mathbf{p}_0^* = (1.0)$ (*black filled circle*) is globally attracting. The focus transition (4.39) occurs at $k_f = 0.0325$ and the saddle-node transition (4.35) at $k_c = 0.04$ *Left*: $k_f < k = 0.035 < k_c$, with $\mathbf{p}_1^*$ and $\mathbf{p}_2^*$ (*red circles*) being a saddle an unstable focus respectively. *Right*: $k_c < k = 0.045$. The *shaded circle* denotes the locus of the attractor relict, the local minimum of $q = \mathbf{f}^2$, see Eq. (4.41), which evolves into the bifurcation point for $k \to k_c$

$$q(\mathbf{x}) \;=\; \mathbf{f}^2(\mathbf{x}), \qquad\qquad \dot{\mathbf{x}} \;=\; \mathbf{f}(\mathbf{x}) \;, \tag{4.41}$$

with q being a measure for the velocity of the flow, which vanishes at a fixpoint.

> Attractor relict. A local, non-zero minimum of $q(\mathbf{x})$, close to a bifurcation point, and turning into a fixpoint at the bifurcation, is denoted an *attractor relict* or a *slow point*.

Beyond the transition, for $k > k_c$, the attractor relict, as indicated in Fig. 4.6, still influences dramatically, on a phenomenological level, the flow. With the attractor relict determining a region in phase space where the direction of the flow turns sharply.

Dynamical Pattern Formation The Gray-Scott system shows a wide range of complex spatio-temporal structures close to the saddle-node line, as illustrated in Fig. 4.7, ranging from dots growing and dividing in a cell-like fashion to more regular stripe-like patterns.

The generation of non-trivial pattern occurs, even though not exclusively, when only the trivial fixpoint $(1,0)$ with the Jacobian

$$A_1 = \begin{pmatrix} -F & 0 \\ 0 & -(F+k) \end{pmatrix} \tag{4.42}$$

is present. There is no way to add a diffusion term A_2, compare expression (4.31), such that $A_1 + A_2$ would have a positive eigenvalue. Pattern formation in the Gray-Scott system is hence not due to a Turing instability.

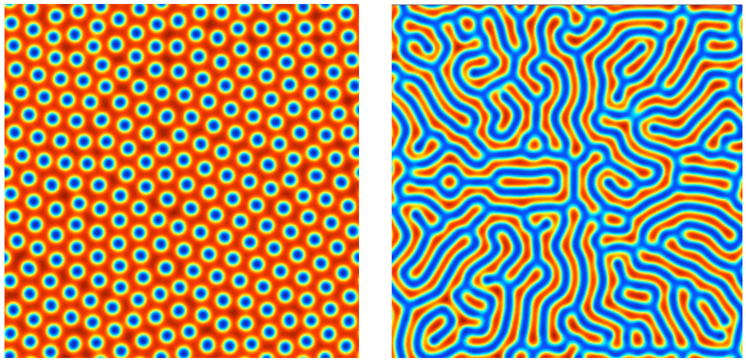

Fig. 4.7 Dynamical patterns for the Gray-Scott model (4.33). Shown is $\rho(x, y, t)$, the diffusion constants are $D_\rho/2 = D_\sigma = 10^{-5}$. The simulation parameters are $(k, F) = (0.062, 0.03)$ (*left*) and $(k, F) = (0.06, 0.037)$ (*right*), as indicated in the phase diagram, Fig. 4.5 (Illustrations courtesy P. Bastani)

4.3 Collective Phenomena and Swarm Intelligence

When a system is composed out of many similar or identical constituent parts, such as the boolean networks discussed in Chap. **??**, their mutual interaction may give rise to interesting phenomena. Several distinct concepts have been developed in this context, each carrying its own specific connotation.

- Collective Phenomena
  Particles like electrons obey relatively simple microscopic equations of motions, like Schrödinger's equation, interacting pairwise. Their mutual interactions may lead to phase transitions and to emergent macroscopic collective properties, like superconductivity or magnetism, not explicitly present in the underlying microscopic description.
- Emergence
  At times loaded heavily by surrounding philosophical discussions, "weak emergence" is equivalent to collective behavior in physics with "strong emergence" denoting the emergence of higher-level properties which cannot be traced back causally to microscopic laws. There is no way, by definition, to use accepted scientific methods to prove or disprove the presence of strong emergence in a given model.
- Self Organization
  When generic generative principles give rise to complex behavior, for a wide range of environmental and starting conditions, one speak of self organization in the context of complex system theory. The resulting properties may be interesting, biologically relevant or emergent.
- Swarm Intelligence
  In biological settings, with the agents being individual animals, one speaks of swarm intelligence whenever the resulting collective behavior is of high

behavioral relevance. Behavior is generically task oriented and swarm intelligence may hence be used algorithmically for solving certain computational problems.

Collective phenomena arise, generally speaking, when “the sum is more than the parts”, just as mass psychology transcends the psychology of the constituent individuals.

4.3.1 Phase Transitions in Social Systems

Phase transitions occur in many physical systems, as further discussed in Chap. **??**, being of central importance also in biology and sociology. A well known psychological phenomenon is, in this context, the transition from normal crowd behavior to collective hysteria. As a simple example we consider here the nervous rats problem.

Calm and Nervous Rats Consider N rats constrained to live in an area A, with a population density $\rho = N/A$. There are N_c calm and N_n nervous rats with $N_c + N_n = N$ and with respective population densities $\rho_c = N_c/A$ and $\rho_n = N_n/A$.

Comfort zone Each rat has a zone $a = \pi r^2$ around it, with r being a characteristic radius. A calm rat will get nervous if at least one nervous rat comes too close, entering its comfort zone a, with a nervous rat calming down when having its comfort zone all for itself.

Master Equation The time evolution for the density of nervous rats is then given by

$$\dot{\rho}_n = P_{c\to n}\,\rho_c \,-\, P_{n\to c}\,\rho_n \,, \tag{4.43}$$

with the transition probabilities

$$P_{c\to n} \,=\, 1-\left(1-\frac{a}{A}\right)^{N_n}, \qquad\qquad P_{n\to c} \,=\, \left(1-\frac{a}{A}\right)^{N-1}\,, \tag{4.44}$$

since $1-a/A$ is the probability for a rat being out of a given comfort zone.

Thermodynamic Limit For constant comfort areas a we consider now the thermodynamic limit $A\to\infty$ and find

$$\lim_{A\to\infty}\left(1-\frac{a}{A}\right)^{\rho_n A} \,=\, \mathrm{e}^{-\rho_n a}, \qquad\qquad \lim_{A\to\infty}\left(1-\frac{a}{A}\right)^{\rho A} \,=\, \mathrm{e}^{-\rho a}$$

for (4.44), where we have used $(N-1)\approx N$, $N_n = \rho_n A$ and $N = \rho A$.

Stationary Solution For the stationary solution $\dot{\rho}_n = 0$ of the master equation (4.43) we then obtain

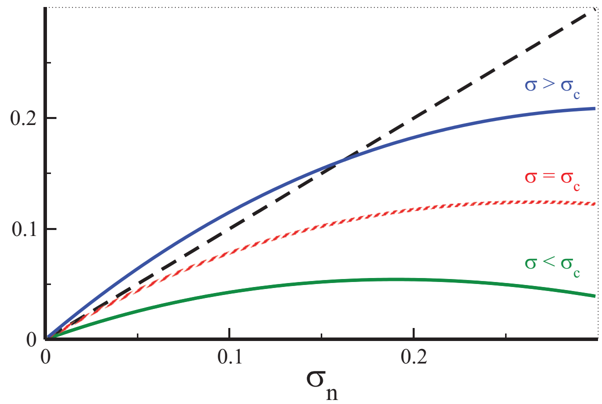

Fig. 4.8 Solution of the nervous rats problem (4.43). Shown is the left- and the right-hand side of the self-consistency condition (4.46), for various number of rats σ in the comfort zone a, as function of the average number of nervous rats σ_n per a. The *dashed line* is σ_n

$$\left(1 - \mathrm{e}^{-\rho_n a}\right)(\rho - \rho_n) = \mathrm{e}^{-\rho a}\rho_n \ , \tag{4.45}$$

which has a trivial solution $\rho_n = 0$ for all population densities ρ and comfort zones a. Multiplying with a we obtain

$$\sigma_n = \mathrm{e}^{\sigma}\left(1 - \mathrm{e}^{-\sigma_n}\right)\ (\sigma - \sigma_n), \qquad \sigma = \rho a, \qquad \sigma_n = \rho_n a \ , \tag{4.46}$$

where the dimensionless densities σ and σ_n correspond to the respective numbers of rats within a comfort area a.

Critical Rat Density The graphical representation of (4.46) is given in Fig. 4.8. A non-trivial solution $\sigma_n > 0$ is possible only above a certain critical number σ_c of rats per comfort zone. At $\sigma = \sigma_c$ the right-hand side of (4.46) has unitary slope, with respect to σ_n, for $\sigma_n \to 0$,

$$1 = \mathrm{e}^{\sigma_c}\,\sigma_c, \qquad \sigma_c \approx 0.56713 \ . \tag{4.47}$$

A finite fraction of nervous rats is present roughly whenever a rat has less than two comfort areas for itself, whereas all rats calm eventually down whenever the average population density ρ is smaller than $\rho_c = \sigma_c/a$. Note, that we could rewrite (4.47) approximatively as

$$\sigma_c = \mathrm{e}^{-\sigma_c} \approx 1 - \sigma_c, \qquad \sigma_c \approx 1/2 \ .$$

4.3.2 Collective Decision Making and Stigmergy

Herding animals and social insects are faced, at time, with the problem of taking decisions collectively. When selecting a new nest for swarming honey bees or a good foraging site for ants, no single animal will compare two prospective target sites. Individual opinions regarding the quality of prospect sites are instead pooled together into groups of alternative decisions with a competitive dynamical process reducing the number of competing opinions until a single target site remains.

Swarming Bees Bees communicate locally by dancing, both when they are in the nest and communicate prospective foraging sites and when a new queen leaves the old nest together with typically about 10.000 workers, searching for a suitable location for building a new nest.

The swarm stays huddled together with a small number of typically 5% of bees scouting in the meantime for prospective new nest sites. Scouts coming back to the swarm waiting site will advertise new locations they found with, with the duration of the dance being proportional to the estimated quality of the prospective nest location.

New scouts ready to fly out observing the dancing returning scouts have hence a higher probability to observe the advertisement of a high quality site and to follow suit. This mechanism leads to a competitive process with lower quality prospective nest sites receiving fewer consecutive visits by the scouts.

Opinion pooling is inherent in this process as there are many scout bees flying out for site inspection and the whole consensus process is an extended affair, taking up to a few days.

Foraging Ants Most social animals gain in survival efficiency by making collective decisions for selected key tasks. An ant colony profits from exploiting the richest food sources available and the corresponding decision problem is illustrated in Fig. 4.9.

The quality of a food resource is given by its distance to the nest and its utility for the species. When the ant returns to the nest it lays down a path of pheromones, with the amount of pheromone released being proportional to the quality of the food site discovered.

Ants leaving the nest in the search for food will tend to follow the pheromone gradient and such arrive predominantly to high quality food sites. Returning they will reenforce the existing pheromone path with an intensity appropriate to their own assessment of the food site. With a large number of ant going forth and back this process will lead to an accurate weighting of foraging sites, with the best site eventually winning in the end over all other prospective food resources.

Information Encoding and Stigmergy Bees and ants need an observable scalar quantity in order to exchange information about the quality of

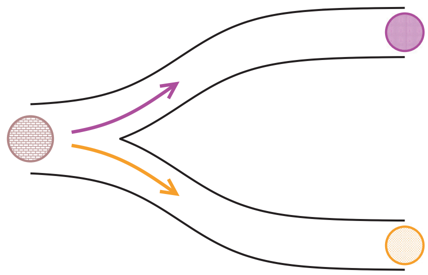

Fig. 4.9 Illustration of binary decision making for foraging ants starting from the nest (*to the left*) and needing to decide which of the (*upper/lower*) food sources may be more profitable

prospective sites. This quantity is time for the case of bees and pheromone intensity for the ants.

Stigmergy. When information is off-loaded to the environment for the purpose of communication one speaks of *stigmergy*.

Producing pheromone traces ants manipulate the environment for the purpose of information exchange.

Ant and Pheromone Dynamics For the binary decision process of Fig. 4.9 we denote with $\rho_{1,2}$ the densities of travelling ants along the two routes, with $\varphi_{1,2}$ and $Q_{1,2}$ the respective pheromone densities and site qualities. The process

$$\begin{aligned} T\dot{\rho}_1 &= (\rho - \rho_1)\varphi_1 - \Psi \qquad & \dot{\varphi}_1 &= -\Gamma\varphi_1 + Q_1\rho_1 \\ T\dot{\rho}_2 &= (\rho - \rho_2)\varphi_2 - \Psi \qquad & \dot{\varphi}_2 &= -\Gamma\varphi_2 + Q_2\rho_2 \end{aligned} \tag{4.48}$$

then describes the dynamics of $\rho = \rho_1 + \rho_2$ ants foraging with T setting the real-world time needed for the foraging and Γ being the pheromone decay constant. The update rates $\dot{\rho}_i$ for the individual number of ants in (4.48) are relative to an average update rate Ψ/T.

Ant Number Conservation The updating rules $\dot{\rho}_{1,2}$ for the ant densities are selected to be conserving with the overall number $\rho = \rho_1 + \rho_2$ of ants remaining constant. This can be achieved by selecting the flux Ψ in (4.48) appropriately as

$$\begin{aligned} 2\Psi &= \rho(\varphi_1 + \varphi_2) - \rho_1\varphi_1 - \rho_2\varphi_2 \qquad & 2T\dot{\rho}_1 &= \rho_2\varphi_1 - \rho_1\varphi_2 \\ &= \rho_2\varphi_1 + \rho_1\varphi_2 & 2T\dot{\rho}_2 &= \rho_1\varphi_2 - \rho_2\varphi_1 \end{aligned} , \tag{4.49}$$

by demanding $\dot{\rho}_1 + \dot{\rho}_2$ to vanish.

Pheromone Conservation Considering with $\Phi = Q_2\varphi_1 + Q_1\varphi_2$ a weighted pheromone concentration we find

$$\dot{\Phi} = -\Gamma\Phi + Q_1Q_2(\rho_1+\rho_2), \qquad \Phi \;\to\; \rho\, Q_1Q_2/\Gamma \;,$$

when using (4.48). Any initial weighted pheromone concentration Φ will hence relax fast to $\rho Q_1Q_2/\Gamma$ and it is hence enough to consider the time evolution in subspace spanned by $\varphi_2 = (\Phi - Q_2\varphi_1)/Q_1$,

$$\begin{array}{rl} 2T\dot{\rho}_1 &= (\rho-\rho_1)\varphi_1 - \rho_1(\Phi - Q_2\varphi_1)/Q_1 \\ \dot{\varphi}_1 &= -\Gamma\varphi_1 + Q_1\rho_1 \end{array} . \tag{4.50}$$

Binary Decision Making There are two fixpoints of the system (4.50), given by

$$\rho_1 = \rho, \qquad \rho_2 = 0, \qquad \varphi_1 = Q_1\rho/\Gamma, \qquad \varphi_2 = 0 \;,$$

and viceversa with $1 \leftrightarrow 2$. The Jacobian of (4.50) for the fixpoint $\rho_1 = 0 = \varphi_1$ is

$$\begin{pmatrix} -\Phi/Q_1 & \rho \\ Q_1 & -\Gamma \end{pmatrix}, \qquad \Delta = \Phi\Gamma/Q_1 - Q_1\rho = (Q_2 - Q_1)\rho \;,$$

when setting $2T = 1$ for simplicity. The trace $-(\Gamma + \Phi/Q_1)$ of the Jacobian is negative and the fixpoint is hence stable/unstable (a saddle), compare (4.25), when the determinant Δ is positive/negative, hence when $Q_2 > Q_1$ and $Q_1 > Q_2$ respectively.

The dynamics (4.50) hence leads to binary decision process with all ants following, in the stationary state, the path with the higher quality factor Q_j.

Ant Colony Optimization Algorithm One can generalize (4.49) to a network of connections with the quality factors Q_i being proportional to the inverse travelling times. This setup is then denoted the *ant colony optimization algorithm*, it has a close connection to the travelling salesman problem. It can be used to find shortest paths on networks.

4.3.3 Collective Behavior and Swarms

Consider a large group of moving agents, like a flock of birds in the air, a school of fishes in the ocean or cars on a motorway, with each agent individually adapting its proper velocity according to the perceived positions and movements of other close-by agents. For modelling purposes one can consider the behavior of the individual agents, as we will do. Alternatively, for a large enough number of agents one may also use a hydrodynamic description by considering a master equation for the density of agents.

Individual Decision Making The members of the swarm take their decisions individually and no group consensus mechanism is in place determining the overall direction the swarm is flying. The resulting group behavior may

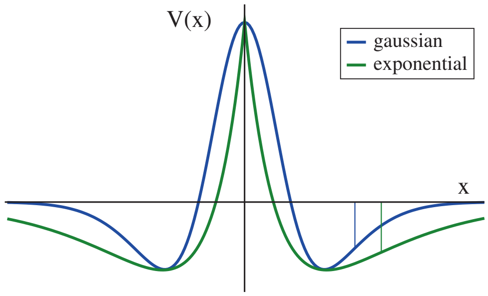

Fig. 4.10 Examples of two typical Mexican hat potentials (4.52), as generated by superposing two Gaussian or two exponentials. The *thin vertical lines* indicate the respective positions of maximal slope

nevertheless have high biological relevance, such as avoiding a predator collectively.

Newton's Equations for Birds The motions for $i = 1, \ldots, N$ birds with positions $\mathbf{x}_i$ and velocities $\mathbf{v}_i$ can be modelled typically by

$$\dot{\mathbf{x}}_i = \mathbf{v}_i \qquad \begin{aligned} \dot{\mathbf{v}}_i = &\ \gamma\big[(v_i^0)^2 - (\mathbf{v}_i)^2\big]\mathbf{v}_i \\ &+ \textstyle\sum_{j\neq i} \mathbf{f}(\mathbf{x}_j, \mathbf{x}_i) + \sum_{j\neq i} \mathbf{g}(\mathbf{x}_j, \mathbf{x}_i|\mathbf{v}_j, \mathbf{v}_i) \end{aligned} \quad , \tag{4.51}$$

with the first term in $\dot{\mathbf{v}}_i$ modelling the preference for moving with a preferred velocity v_i^0. The collective behavior is generated by the pairwise interaction terms $\mathbf{f}$ and $\mathbf{g}$. Reacting to observations needs time and time delays are inherently present in $\mathbf{f}$ and $\mathbf{g}$.

Distance Regulation Animals dispose of preferred distances to their neighbors (to the side, front, back, above and below) and $f(\mathbf{x}_j, \mathbf{x}_i)$ may be taken, as a first approximation, as the derivative of a "Mexican hat potential" $V(z)$,

$$\begin{aligned} f(\mathbf{x}_j, \mathbf{x}_i) = f(\mathbf{x}_j - \mathbf{x}_i) &= -\nabla V(|\mathbf{x}_j - \mathbf{x}_i|) \\ V(z) &= A_1\kappa(z/R_1) - A_2\kappa(z/R_2) \end{aligned} \ , \tag{4.52}$$

where $\kappa(z)$ is a function decaying, for example, as an exponential $\sim \exp(-z)$, as a Gaussian $\sim \exp(-z^2)$, or as a powerlaw $\sim 1/z^\alpha$. For suitable selections of the amplitudes A_i and of the characteristic distances R_i the potential is repelling at short distances together with stable symmetric minima, as illustrated in Fig. 4.10

Alignment of Velocities The function $\mathbf{g}(\mathbf{x}_j, \mathbf{x}_i|\mathbf{v}_j, \mathbf{v}_i)$ in (4.51) expresses the tendency to align one's own velocity with the speed and the direction of the movement of other nearby members of the flock. A suitable functional form would be

$$\mathbf{g}(\mathbf{x}_j, \mathbf{x}_i|\mathbf{v}_j, \mathbf{v}_i) = \big(\mathbf{v}_j - \mathbf{v}_i\big)A_v\kappa(|\mathbf{x}_j - \mathbf{x}_i|/R_v) \ , \tag{4.53}$$

with the tendency to align vanishing both for identical velocities $\mathbf{v}_j$ and $\mathbf{v}_i$ and for large inter-agent distances $|\mathbf{x}_j - \mathbf{x}_i| \gg R_v$.

Hiking Humans Equations like (4.51) describe nicely the observed flocking behavior of birds and schools of fishes. We may ask when a group of humans hiking along a one-dimensional trail will break apart due to differences in the individual preferred hiking speeds v_i^0?

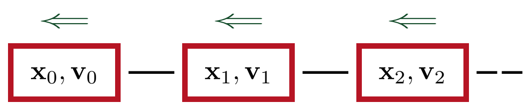

The distance alignment force $\mathbf{f}$ is normally asymmetric, we assume here that walkers pay attention only to the person in front. The group then stays together, for the case that $\mathbf{f}$ vanishes and that all other $v_i < v_0$, if everybody walks with the speed $v \equiv v_0$ of the leader. The restraining potential illustrated in Fig. 4.10 has a maximal slope f_{max} and the maximal individual speed difference $v_0 - v_i$ is then determined through

$$\gamma\big[(v_i^0)^2 - (v)^2\big]v = -f_{max}, \qquad (v_i^0)^2 = (v)^2 - f_{max}/(\gamma v) \ .$$

The group is more likely to break apart when the desire γ to walk with one's own preferred velocity v_i^0 is large.

4.3.4 Opinion Dynamics

In opinion dynamics research one considers agents have real-valued opinions x_i which may change through various processes, like conviction or consensus building.

Bounded Confidence We consider a basic process for consensus building. Two agents (x_i, x_j) meeting agree on the consensus opinion $\bar{x}_{ij} = (x_i + x_j)/2$ when their initial opinions are not too different,

$$(x_i, x_j) \quad \to \quad \begin{cases} (\bar{x}_{ij}, \bar{x}_{ij}) & \text{if } |x_i - x_j| < d \\ (x_i, x_j) & \text{if } |x_i - x_j| > d \end{cases} \ . \tag{4.54}$$

They do not agree to a common opinion if they initially differ beyond the confidence bound d and distinct sets of attracting opinions tend to form, as illustrated in Fig. 4.11.

Master Equation For large populations of agents we may define with $\rho(x, t)$ the density of agents having opinion x, with the time evolution given by the master equation

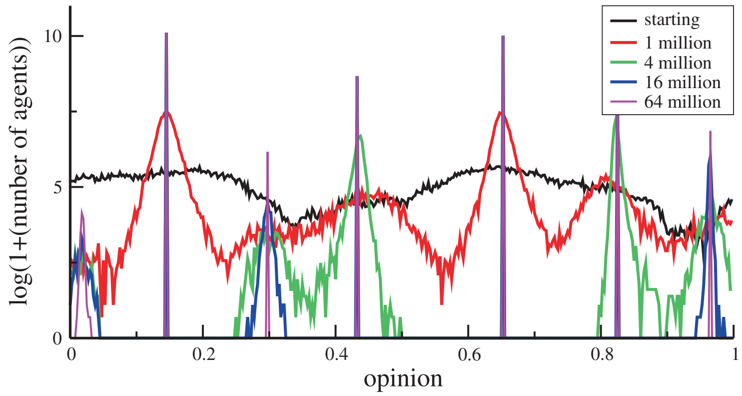

Fig. 4.11 For a confidence interval $d = 0.1$ a simulation of 60,303 agents with $1 \cdot 10^6$, $4 \cdot 10^6$, $16 \cdot 10^6$ and $64 \cdot 10^6$ pairwise updatings of type (4.54). Opinion attractors with a large number of supporters tend to stabilize faster than attracting states containing smaller number of agents

$$\tau \dot{\rho}(x) = 2 \int_{-d/2}^{d/2} \rho(x+y)\rho(x-y)dy \; - \; \int_{-d}^{d} \rho(x)\rho(x+y)dy \;, \tag{4.55}$$

with τ setting the time scale of the consensus dynamics and with the time dependency of $\rho(x,t)$ being suppressed. The first term results from two agents agreeing on x, the second term describes the flow of agents leaving opinion x by agreeing with other agents within the confidence interval d.

Infinitesimal Confidence It is possible to turn (4.55) into an ordinary differential equation by considering the limit $d \to 0$ via a Taylor expansion

$$\rho(x+y) \approx \rho(x) \; + \; \rho'(x)y \; + \; \rho''(x)\frac{y^2}{2} \; + \; \ldots \; . \tag{4.56}$$

Substituting (4.56) into (4.55) one notices that the terms proportional to y^0 cancel, as the overall number of agents is conserved. The terms $\sim y^1$ also vanish due to symmetry and we obtain

$$\begin{aligned}
\tau \dot{\rho} &= 2 \int_{-d/2}^{d/2} \left[\rho\rho'' - (\rho')^2\right] y^2 dy \; - \; \rho\rho'' \int_{-d}^{d} \frac{y^2}{2} dy \\
&= 4 \left[\rho\rho'' - (\rho')^2\right] \frac{1}{3}\frac{d^3}{8} \; - \; \rho\rho''\frac{d^3}{3} = -\frac{d^3}{6} \cdot \left[\rho\rho'' + (\rho')^2\right]
\end{aligned}$$

Using $\partial^2\rho^2/\partial^2 x = 2[\rho'\rho' + \rho\rho'']$ we find

$$\frac{\partial \rho}{\partial t} = -\frac{d^3}{12\tau}\frac{\partial^2 \rho^2}{\partial^2 x}, \qquad \dot{\rho} = -D_o \Delta \rho^2 \;, \tag{4.57}$$

with Δ denoting the dimensional Laplace operator, here in one dimension. ρ^2 enters the evolution equation as two agents have to interact for the dynamics to proceed.

One can keep $D_o = d^3/(12\tau)$ in (4.57) constant in the limit $d \to 0$ by appropriately rescaling the time constant τ, in analogy to the derivation of the diffusion equation $\dot{p} = D\Delta p$ discussed in Sect. **??**.

Opinion Current Recasting (4.57) in terms of the continuity equation

$$\dot{\rho} + \nabla \cdot \mathbf{j}_o = 0, \qquad \mathbf{j}_o = D_o \nabla \rho^2 \, , \tag{4.58}$$

defines the opinion current $\mathbf{j}_o$. With D_0 and ρ being positive this implies that the current strictly flows uphill, an example of a "rich gets richer dynamics" which is evident also in the simulation shown in Fig. 4.11.

4.4 Car Following Models

The flow of cars on a motorway can be modelled by *car following models*, akin to the bird flocking model discussed in Sect. 4.3.3, with the velocity dependent forces being of central importance together with an appropriate incorporation of human reaction times.

Chain of Cars We denote with $x_j(t)$ the position of the cars $j = 0, \ldots$ on the one-dimensional motorway, with the acceleration $\ddot{x}_j$ given by

$$\ddot{x}_{j+1}(t+T) = \sum_{j \neq i} g(x_j, x_i | \dot{x}_j, \dot{x}_i) = \lambda \big[\dot{x}_j(t) - \dot{x}_{j+1}(t)\big] \, , \tag{4.59}$$

with λ being a reaction constant and T the reaction time. A driver tends to break when moving up to the car in the front and to accelerate when the distance grows. In car following models, using the notation of (4.51), one considers mostly velocity-dependent forces.

4.4.1 Linear Flow and Carrying Capacity

One of the first questions for traffic planning regards the maximal number q of cars per hour, the carrying capacity of a road. In the optimal situation all car advance with identical velocities u and one would like to evaluate $q(u)$.

Carrying Capacity for the Linear Model We denote with s the distance between two cars. Integrating the linear model (4.59), and assuming the steady-state conditions $\dot{x}_j \equiv u$ and $x_j - x_{j+1} \equiv s$, one obtains

$$\dot{x}_{j+1} = \lambda[x_j - x_{j+1}] + c_0, \qquad u = \lambda(s - s_0) \ , \tag{4.60}$$

where we have written the constant of integration as $c_0 = -\lambda s_0$, with s_0 being the minimal allowed distance between the cars. The carrying capacity q, the number of cars per time passing, is given by the product of the mean velocity u and the density $1/s$ of cars,

$$q = \frac{u}{s} = \lambda\left(1 - \frac{s_0}{s}\right) = \frac{u}{s_0 + u/\lambda}, \qquad s = s_0 + \frac{u}{\lambda} \ , \tag{4.61}$$

where we have expressed q either as a function of the inter-vehicle distance s or as a function of the mean velocity u. Above expression would result in a carrying capacity being maximal for empty streets with $s \to \infty$ and dropping monotonically to zero when the maximal density $1/s_0$ of cars is reached.

Maximal Velocity The linear model (4.59) cannot be correct, as the velocity $u = \lambda(s - s_0)$, as given by (4.60), would diverge for empty highways with large inter-vehicle distances $s \to \infty$. Real-world cars have however an upper velocity u_{max} and the carrying capacity must hence vanish as u_{max}/s for large inter-vehicle spacings s.

A natural way to overcome this deficiency of the basic model (4.59) would be to consider terms, like for the bird flocking model (4.51), expressing the preference to drive with a certain velocity. An alternative venue, pursued normally when modelling traffic flow, is to consider non-trivial distance dependencies within the velocity dependent force $g(x_j, x_i|\dot{x}_j, \dot{x}_i)$.

Non-Linear Model Driving a car one reacts stronger when the car in front is closer, an observation which can be modelled via

$$\ddot{x}_{j+1}(t+T) = \lambda\,\frac{\dot{x}_j(t) - \dot{x}_{j+1}(t)}{[x_j(t) - x_{j+1}(t)]^{1+\alpha}}, \qquad \alpha > 0 \ , \tag{4.62}$$

when assuming a scale-invariant dependency of the reaction strength. Integrating (4.62) one obtains, in analogy to (4.60),

$$\dot{x}_{j+1} = \frac{\lambda}{-\alpha}[x_j - x_{j+1}]^{-\alpha} + d_0, \qquad u = \frac{\lambda}{\alpha}\left[\frac{1}{s_0^\alpha} - \frac{1}{s^\alpha}\right] \ , \tag{4.63}$$

with s_0 denoting again the minimal inter vehicle distance and $d_0 = \lambda/(\alpha s_0^\alpha)$. For $\alpha > 0$ the mean velocity u now takes a finite value

$$u_{max} = \frac{\lambda}{\alpha s_0^\alpha}, \qquad u = u_{max} - \frac{\lambda}{\alpha s^\alpha}, \qquad \frac{1}{s} = (u_{max} - u)^{1/\alpha}\left(\frac{\alpha}{\lambda}\right)^{1/\alpha}$$

for near to empty streets with $s \to \infty$. The carrying capacity $q = u/s$ is then given by the parabola

$$q(u, \alpha = 1) = u(u_{max} - u)/\lambda \tag{4.64}$$

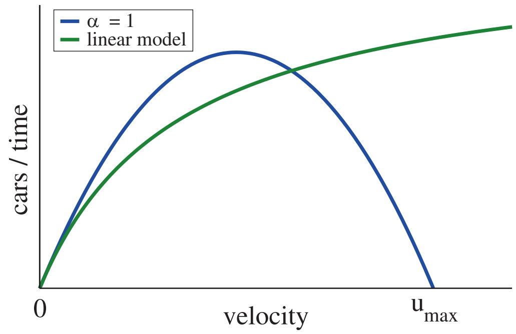

Fig. 4.12 The number of cars per hour passing on a highway for the linear (4.61) and for the non-linear (4.64) car following model. $\lambda = 3$ in both cases. The carrying capacity vanishes when the road is congested and the mean velocity $u \to 0$. Arbitrary large cruising velocities are possible for the linear model when the street is empty

for $\alpha = 1$, as illustrated in Fig. 4.12. The traffic volume is maximal for an intermediate mean velocity u, in accordance with daily observations.

4.4.2 Self-Organized Traffic Congestions

A steady flow of cars with $\dot{x}_j(t) \equiv u$ may be unstable due to fluctuations propagating along the line of vehicles, a phenomena possibly inducing traffic congestion even in the absence of external influences, such as an accident.

Moving frame of reference The linear car following model (4.59) is the minimal model for analyzing the dynamics for intermediate to high densities of vehicles. We are interested in the evolution of the relative deviations $z_j(t)$ from the steady state,

$$\dot{x}_i(t) = u\big[1 - z_i(t)\big], \qquad \dot{z}_{j+1}(t+T) = \lambda\big[z_j - z_{j+1}\big] \tag{4.65}$$

and will consider with (4.65) the evolution equations in the moving frame of reference.

Slow Perturbations We assume that the leading car changes its cruising speeds via

$$z_0(t) \;\to\; \mathrm{e}^{\gamma t}, \qquad \gamma = 1/\tau + i\omega \qquad \tau > 0\ . \tag{4.66}$$

For evaluating the exact time evolution of the following cars one would need to integrate piecewise (4.65), as explained in Sect. **??**, consecutively for the intervals $t \in [nT, (n+1)T]$.

The timescale of the perturbation (4.66) to grow is τ and the system will follow the behavior of the lead car relatively smooth if the delay interval T is substantially smaller, which we will assume here.

Recursion We assume that all cars follow the time evolution (4.66) with amplitudes a_j,

$$z_j(t) = a_j\, e^{\gamma t}, \qquad \gamma \mathrm{e}^{\gamma T} a_{j+1} = \lambda(a_j - a_{j+1}) \ .$$

Solving for a_{j+1} we obtain the linear recursion

$$a_{j+1} = \frac{\lambda}{\lambda + \gamma \mathrm{e}^{T\gamma}}\, a_j, \qquad a_n = \left(\frac{\lambda}{\lambda + \gamma \mathrm{e}^{T\gamma}}\right)^n a_0 \ . \tag{4.67}$$

The recursion is stable for real exponents $\gamma = 1/\tau$.

Delay Induced Instabilities We consider harmonic oscillations of the lead car velocity corresponding to imaginary exponents $\gamma = i\omega$ in (4.66). Evaluating the norm

$$\left|\lambda + \gamma \mathrm{e}^{T\gamma}\right|^2 = \left|\lambda + i\omega \mathrm{e}^{iT\omega}\right|^2 = \left[\lambda - \omega \sin(T\omega)\right]^2 + \omega^2 \cos^2(T\omega)$$

we obtain

$$\left|\frac{\lambda}{\lambda + \gamma \mathrm{e}^{T\gamma}}\right| = \left(\frac{\lambda^2}{\lambda^2 + \omega^2 - 2\lambda\omega \sin(T\omega)}\right)^{1/2} \tag{4.68}$$

for the norm of the prefactor in the recursion (4.67). The recursion is then unstable if

$$\lambda^2 + \omega^2 - 2\lambda\omega \sin(T\omega) \ < \ \lambda^2, \qquad \omega \ < \ 2\lambda \sin(T\omega) \ . \tag{4.69}$$

Suitable large time delays, with $T\omega \approx \pi/2$, induce an instability for any values of λ and ω, in accordance with our discussion in Sect. **??** regarding the influence of time delays in ordinary differential equations.

Self-Organized Traffic Jams An instability occurs also in the limit of infinitesimal small frequencies $\omega \to 0$, when

$$1/(2\lambda) \ < \ T, \qquad \sin(T\omega) \approx T\omega \ . \tag{4.70}$$

Strong (λ large) and slow (T large) reactions of drivers are hence more likely to induce self-organized traffic jams.

Propagating Perturbations We consider a slowly growing perturbation with real $\gamma = 1/\tau$ inducing deviations $z_n(t)$ from the steady state, with

$$z_n(t) \ = \ a_0\, C^n\, \mathrm{e}^{t/\tau} \ = \ a_0\, \mathrm{e}^{n \log(C)}\, \mathrm{e}^{t/\tau}, \qquad C = \frac{\lambda\tau}{\lambda\tau + \mathrm{e}^{T/\tau}}.$$

We are interested in the propagation speed v of the perturbation, along the line of cars, as defined by

$$z_n(t) \;=\; a_0\,\mathrm{e}^{(n-vt)\log(C)}, \qquad\qquad v \;=\; \frac{-1}{\tau\log(C)}\;. \tag{4.71}$$

The speed is positive, $v > 0$, since $0 < C < 1$ and $\log(C) < 0$. Large reaction times T limit the propagation speed, since

$$\log(C) \;\to\; -T/\tau, \qquad\qquad v \;\to\; 1/T$$

in the limit $T \gg \tau$.

Exercises

Instability of Euler's method

Euler's method is in general not suitable for numerically integrating partial differential equations. Discretizing in space and time the diffusion equation (4.1) reads

$$\frac{\rho(x,t+\Delta t)-\rho(x,t)}{\Delta t} = D\,\frac{\rho(x+\Delta x,t)+\rho(x-\Delta x,t)-2\rho(x,t)}{(\Delta x)^2}$$

in one dimension. Prove that the resulting explicit time evolution map becomes unstable for $D\Delta t/(\Delta x)^2 > 1/2$ by considering $\rho(x,0)=\cos(\pi x/\Delta x)$ as a particular initial state.

Exact propagating wavefront solution

Find the reaction-diffusion system (4.2) for which the Fermi function

$$\rho^*(x,t) = \frac{1}{1+\mathbf{e}^{\beta(x-ct)}}$$

is an exact particular solution for a solitary propagating wavefront. Determine the reaction term $R(\rho)$ by evaluating the derivatives of ρ^*, consider appropriate special values for β and the propagation velocity c.

Linearized Fisher equation

Consider the modified reaction-diffusion system

$$\dot\rho = \rho(1-\rho)+\rho''+\frac{2}{1-\rho}(\rho')^2 \tag{4.72}$$

and show that it is equivalent to the linearized Fisher equation (4.18) using the transformation $\rho = 1-1/u$.

Turing instability with two stable nodes

Is it possible that the matrix A_1 entering the Turing instability and defined in (4.26), with positive $\epsilon_a, \epsilon_b > 0$, describes a stable node with both $\lambda_\pm < 0$? If yes, show that the superposition of two stable nodes may generate an unstable direction.

Eigenvalues of 2×2 matrices

Use the standard expression (4.25) for the eigenvalues of a 2×2 matrix and show that local maxima of the potential $V(x)$ of a one-dimensional mechanical system

$$\dot{x} = y, \qquad \dot{y} = -\lambda(x)y - V'(x)$$

with a space-dependent damping factor $\lambda(x)$ are always saddles.

Large densities of nervous rats

Evaluate, using the stationarity condition (4.46), the number of nervous rats σ_n per comfort zone for large values of σ. When do all rats become nervous?

Agents in the bounded confidence model

Show that the total number of agents $\int \rho(x)dx$ is conserved for the bounded confidence model (4.55) for opinion dynamics.

Further Reading

You are encouraged to take a look at Murray (1993) and Ellner et al. (2011) for classical and modern in-depth treatises on mathematical modelling in biology and ecology, at Cross et al. (2009) for the generic mathematics of pattern formation in reaction-diffusion systems and to Petrovskii et al. (2010) for a discussion of exactly models in this field. Fascinating pictures for the Gray-Scott reaction diffusion system can be found additionally in Pearson (1993).

We further suggest Bonabeau et al. (1990) for a classics on swarm intelligence, Kerner (2004) for traffic modelling and Castellano (2002) for a review on opinion dynamics and flocking behaviors.

References

Bonabeau, E., Dorigo, M., Theraulaz, G.1990 *Swarm intelligence: from natural to artificial systems.*Oxford University Press.

Castellano, C., Fortunato, S., and Loreto, V. 2009 Statistical physics of social dynamics. *Review of Modern Physics* **81**, 591.

Cross, M., Greenside, H.2009 *Pattern Formation and Dynamics in Nonequilibrium Systems.* Cambridge University Press.

Ellner, S.P., Guckenheimer, J.2011 *Dynamic Models in Biology.* Princeton University Press.

Kerner, B.S. 2004 *The physics of traffic: empirical freeway pattern features, engineering applications, and theory.* Springer, Berlin.

Murray, J.D. 1993 *Mathematical Biology.* Springer, Berlin.

Pearson, J.E. 1993 Complex patterns in a simple system. *Science* **261**, 189–192.

Petrovskii, S.V., Bai-Lian L.2010 *Exactly solvable models of biological invasion.*CRC Press.